Selective Sorption

DOI: 10.1002/anie.201307656

Shape Selectivity by Guest-Driven Restructuring of a Porous Material**

*J. E. Warren, C. G. Perkins, K. E. Jelfs, P. Boldrin, P. A. Chater, G. J. Miller, T. D. Manning, M. E. Briggs, K. C. Stylianou, J. B. Claridge, and M. J. Rosseinsky**

Abstract: *A flexible metal-organic framework selectively sorbs para- (pX) over meta-xylene (mX) by synergic restructuring around pX coupled with generation of unused void space upon mX loading. The nature of the structural change suggests more generally that flexible structures which are initially mismatched in terms of fit and capacity to the preferred guest are strong candidates for effective molecular separations.*

Porous materials are widely used in shape-selective sorption.[1] Metal-organic frameworks (MOFs) have chemically tailorable internal surfaces[2] bearing a wide range of functional groups and can respond flexibly[3] to guest uptake.[4,5] Shape selectivity is achieved in rigid porous hosts by matching their fixed channel geometries to the target molecule.[6] MOFs are attractive for a range of separation applications[1,7] because of electronic[8] and geometrical features that are hard to access in other classes of porous crystalline materials.[9] Flexible MOFs display excellent figures of merit for CO_2/CH_4[10] and N_2/CO separations.[11] The separation of the xylene and ethylbenzene C_8 isomers has been demonstrated by zeolites[12] and by rigid MOFs.[13] Flexible MOFs can also perform this separation in vapor[14] and liquid phases,[15] and undergo "breathing"-type structural changes when sorbing C_8 isomers,[16] but currently show lower selectivities than rigid hosts. We present a flexible MOF that differentially restructures around *para*- (pX) and *meta*-xylene (mX) to achieve high selectivity, and demonstrate how the restructuring distinguishes between the two isomers at the atomic level.

$[Ce(HTCPB)\cdot(EtOH)_{0.28}(H_2O)_{2.75}]$ (**1**; Figure 1; see also the Supporting Information, Figures S1–6),[17] was synthesized by solvothermal reaction of $Ce(NO_3)_3$ with the tetradentate carboxylic acid H_4TCPB[18] in $EtOH/H_2O$, with incomplete deprotonation of the linker. The rectangular linker affords a large channel 1 containing the ethanol guests and a smaller channel 2 containing water (Figure 1 c,f). [Ce(HTCPB)] (**3**) is accessed by desolvation of **1** (Figures 1 and S7–9), is permanently porous[19] to CO_2 and N_2, and displays a reversible water sorption isotherm (Figures S10 and S11). The defining structural units of **1** are Ce_2 dimers, formed by four bridging carboxylates (from carboxyphenyl rings 4 and 5 of the linker), and coordinated terminally by non-bridging protonated COOH (from carboxyphenyl ring 1) and carboxylate (from carboxyphenyl ring 2), plus EtOH and H_2O ligands (Figure 1 a). These dimers are connected into sheets through the HTCPB molecule, but isolated from dimers in adjacent sheets by the capping H_2O and EtOH ligands. Compound **3** is formed in a stepwise desolvation process (via an unusual intermediate, **2**), in which both of these ligands are substituted by the carboxylate on carboxyphenyl ring 2, which now bridges two neighboring dimers (Figure 1 b) to link the sheets in three dimensions (Figure 1 d). This requires reorientation of the HTCPB linker with the rotation of carboxyphenyl ring 2 (Table S2), and reorients the dimers in **3** to align their Ce–Ce vector more closely to the channel direction (Table S3), thus opening up channel 2 (Figure 1 f,g). Hydrogen atoms at the 3 and 6 positions of the central benzene ring project into channel 1, with channel 2 decorated by hydrogen

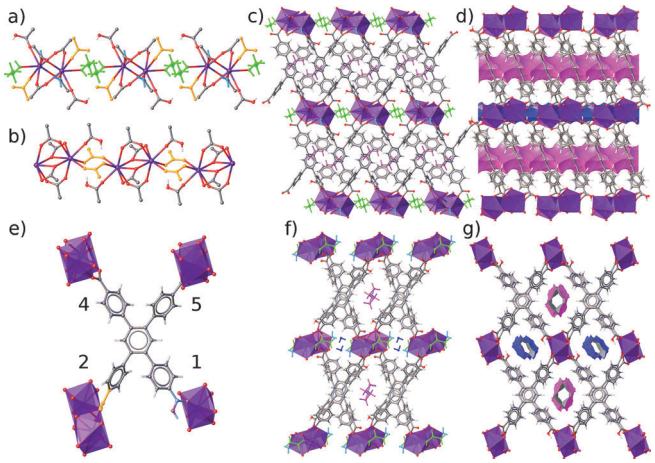

Figure 1. Structures of **1** and **3**. a) Coordination environment of Ce in **1**: coordinated EtOH and H_2O shown in green and cyan, respectively; the purple Ce centers form carboxylate-bridged dimers; the non-bridging carboxylate on carboxyphenyl ring 2 orange; C gray, O red, H white. b) Coordination environment of Ce in **3**; the carboxylates on carboxyphenyl ring 2 connect the dimers. c) View along [010] of **1**, Ce coordination environment shown as purple polyhedra. d) View along [010] of **3**: the carboxyphenyl ring 2 carboxylate connects the Ce dimers; Channel 1 magenta, channel 2 blue. e) Connectivity of the HTCPB ligand viewed normal to the central benzene ring plane in **3** with pendant ring numbering (Figure S8 is the parallel view; Figure S6 shows equivalent views of **1**). f) **1** viewed along [100], with channel EtOH magenta, H_2O dark blue. g) View of **3** along [100].

[*] Dr. J. E. Warren, C. G. Perkins, Dr. K. E. Jelfs, Dr. P. Boldrin, Dr. P. A. Chater, Dr. G. J. Miller, Dr. T. D. Manning, Dr. M. E. Briggs, Dr. K. C. Stylianou, Dr. J. B. Claridge, Prof. M. J. Rosseinsky
Department of Chemistry, University of Liverpool
Liverpool, L69 7ZD (UK)
E-mail: M.J.Rosseinsky@liverpool.ac.uk
Homepage: http://www.liv.ac.uk/chemistry/research/rosseinsky-group/

[**] We thank the EPSRC for support under EP/H000925. We thank A. McLennan for experimental assistance.

Supporting information for this article is available on the WWW under http://dx.doi.org/10.1002/anie.201307656.

atoms from the four pendant benzoates. Carboxyphenyl ring 1 is unique, as the COOH group coordinates solely to one metal center, with the OH moiety lining channel 2. Compound **3** thus displays a hierarchy of structure-forming bonds, with pore shapes defined by ligand torsions and displacements from **1**, and has channel surfaces comprising a range of functionalities.

To investigate the potential for selective xylene isomer uptake, docking calculations were performed with rigid **3** as a host. These indicated that the topography of the pores permits occupation by pX, while excluding uptake of the similarly sized mX (Figure 2a,b). In the larger channel 1, several positions are available for the guest, with the preferred location defined by the formation of two symmetrical C–H···π interactions[20] from the central benzene ring of the HTCPB ligand of the framework to the pX benzene ring (Figure 2a). The Ce_2 dimer defines a pocket in channel 2 the length of which matches that of pX, with the constriction beyond this pocket defined by the terminal COOH on carboxyphenyl ring 1 preventing occupation of other locations in this channel (Figure 2b). The pX orientation is fixed by the smaller channel 2 dimensions, which from GCMC simulations produce a lower computed occupancy of 13% than the fully occupied channel 1, thus showing that **3** does not have optimized capacity for pX.

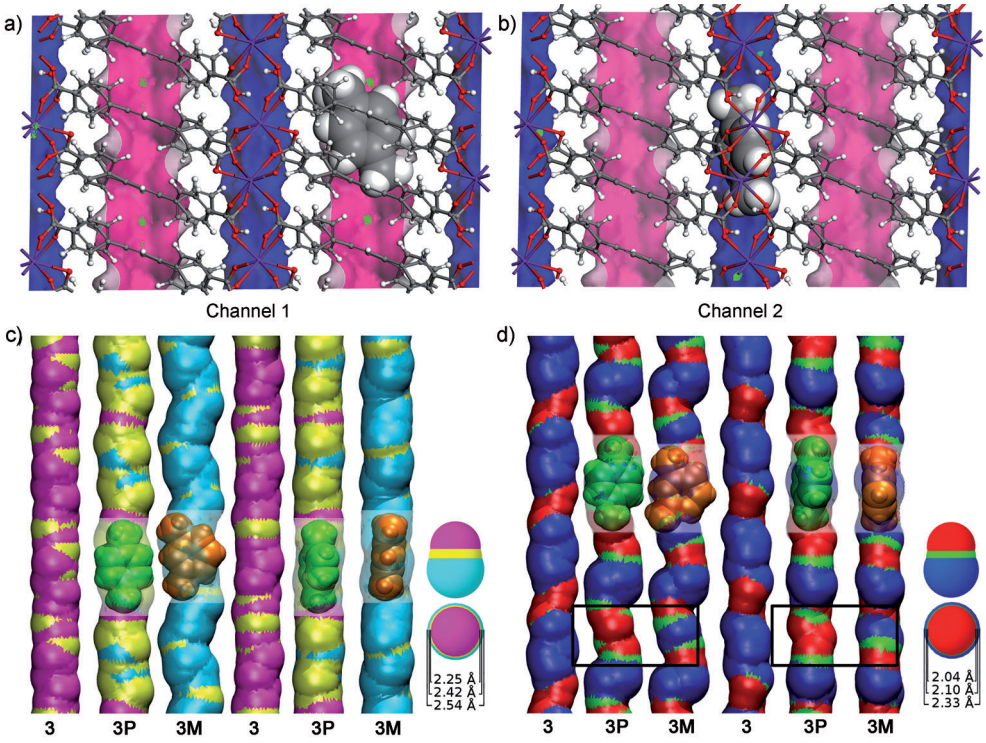

Figure 2. Computed guest locations in rigid **3**, and measured channel relaxation upon guest loading. a) Computation: an energetically favorable docking site in rigid **3** for the pX guest in channel 1 and b) in channel 2; frequently sampled sorption sites at high loading are shown in green, sampled from GCMC (Grand Canonical Monte Carlo) simulations at 10 bar and 383 K (Tables S4,5,7, and Figures S12 and 13). c) Experimental channel surfaces for **3** and xylene-loaded **3P** and **3M** generated by Hole 2[26] (Table S11) for channel 1 and d) channel 2. The black rectangle highlights the guest-free expanded region in **3M** away from the mX guest location, where there is no equivalent expansion in **3P**. Xylene guests (pX green, mX orange) are shown in experimentally determined locations. The coloring of the surface indicates the channel radius at that point. A different set of colors was used to highlight the surfaces of the two channels to avoid uniform coloration of the larger channel 1.

Batch experiments on bulk powder samples in liquid C_8 isomer mixtures established that **3** is selective for the uptake of pX over the other xylene isomers and ethylbenzene (EB) (Figure S16): the selectivities are determined by GC measurements. An α_{pXmX} selectivity of 4.5 (Tables S8–10: kinetic diameters pX 5.8 Å, mX 6.4 Å) was measured. The selectivities for pX over *ortho*-xylene (6.5 Å) and EB (5.8 Å) of 5.6 and 2.4, respectively, are also high.[21] Current pX/mX separation processes use (K, Ba)-exchanged and K-exchanged zeolite Y, for which the selectivity parameter $\alpha_{pXmX} = 4$ and 4.5, respectively.[22] Rigid MOF materials can produce equivalent performance (e.g. MIL-125(Ti)-NH_2 with $\alpha_{pXmX} = 4.4$)[23] based on the same intrapore xylene packing separation mechanism.

The observation that **3** sorbs mX is contrary to the rigid lattice docking predictions, and indicates a flexible structural response to guests. The reasons for this combination of selectivity and flexibility were then identified in single-crystal structure determinations of the [Ce(HTCPB)·(xylene)] phases, denoted **3P** and **3M**, formed by loading pX and mX, respectively, into **3** (Figures S18–S24 and Table S12). Both xylene isomers are adsorbed individually to the same extent, with the observed capacity for pX almost double that computed for rigid **3** because of the guest-driven restructuring of the host. The HTCPB linker pivots about its central benzene ring upon xylene loading to exchange the dimer-forming and -bridging roles of rings 5 and 2 in **3** by correlated motion along the dimer chain, while leaving the Ce coordination intact (Figure 3 and S21).

The channel geometries in **3** and the guest-loaded **3P** and **3M** are shown in Figure 2c,d. In **3**, the larger channel 1 is also more cylindrical than channel 2, which is straight, but pocketed at the dimer positions. Channel 1 largely retains cylindrical character when pX is sorbed to form **3P**, but becomes less regular in diameter with the formation of pockets at the pX guest locations. This is achieved by an

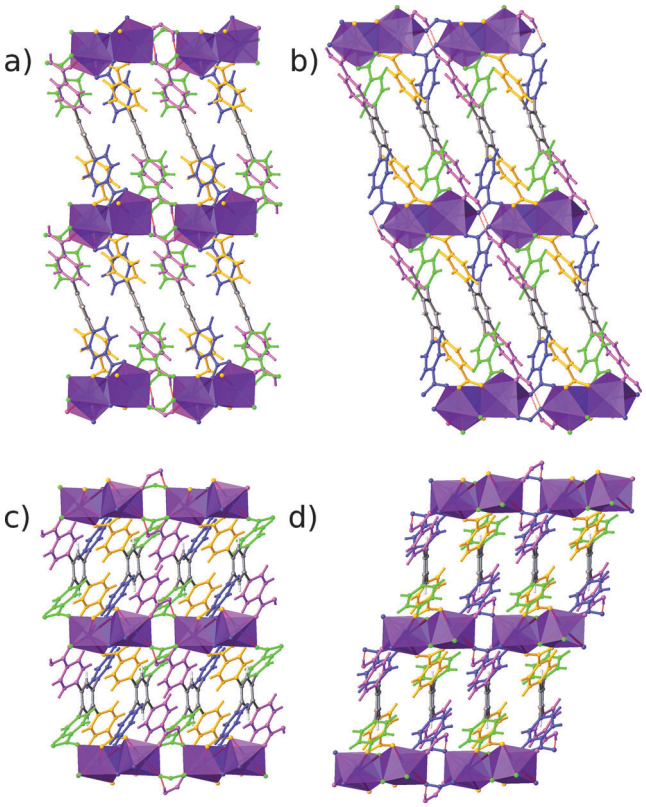

Figure 3. The structural roles of rings 2 and 5 in bridging and forming the Ce_2 dimers are exchanged when **3P** forms from **3** upon xylene loading (the same change occurs upon formation of **3M**); carboxyphenyl ring 1 purple, ring 2 green, ring 4 yellow, ring 5 blue. a) **3** viewed along [010]; the 1,2 edge of the central benzene ring of the ligand is located between the dimers, with carboxyphenyl ring 2 bridging them, and with the 4,5 edge carboxylates forming the dimers. b) **3P** viewed along [010]; each edge of the central benzene now has one group (2 or 4) involved in dimer formation, and one (1 or 5) between the dimers, with 5 bridging. c) **3** viewed along [001]. d) **3P** viewed along [001]. Rotation of the central benzene ring and displacement of successive dimer chains pivots the HTCPB linker about the fixed rings (1 and 4), allowing rings 2 and 5 to change function in **3P**. Figure S21 shows the changes of the carboxylate positions along the dimer chain associated with this transformation.

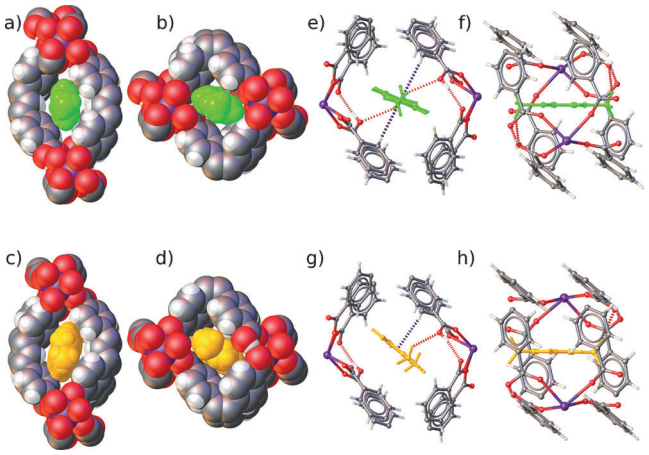

Figure 4. Experimentally determined environments of the xylene guests in **3**. a–d) Space-filling van der Waals (vdW) radii representation of xylene guests (pX green, mX orange) viewed down [100] for channel 1: a) pX in **3P**, c) mX in **3M**; for channel 2: b) **3P**, d) **3M**. e–h) Depiction of pocket surrounding the xylenes in channel 2; C–H···O bonds from xylene to framework and O–H···O from framework to framework are shown as red dotted lines; C–H···π interactions from framework to xylene shown in purple, these are removed for clarity in (f) and (h). e) View down [100] for pX in **3P** and g) mX in **3M**. f) View down the xylene plane with xylene aligned flat for pX in **3P** and h) mX in **3M**. mX disorder removed and only a single position shown for clarity.

expansion (of ca. 0.2 Å) around the larger benzene ring section of the pX guest coupled with narrowing (magenta in Figure 2c) around the smaller methyl groups. This distortion of the host to match the shape of the guest results in crystallographic order of pX in these well-defined locations. In contrast, mX loading expands channel 1 in **3M** to a greater extent (ca. 0.3 Å; cyan in Figure 2c) and imposes a zig-zag geometry on the channel. This more pronounced structural change is required by the angular disposition of the methyl groups in mX, but does not however produce a unique guest position: **3M** has extensive translational positional disorder of mX along the channel.

The long axis of pX aligns with the channel 1 direction in **3P** (Figure 4a), in contrast to the modeled orientation in unrelaxed **3** where this channel is sufficiently wide at the guest location for pX to tilt across it (Figure 2a). This is consistent with relaxation of the channel to optimize the fit between guest and host van der Waals surfaces. The pX position is defined by two symmetrical C–H···π interactions on both faces of the guest with the hydrogen atoms of the HTCPB central benzene ring (Figures S24–26, and Tables S13 and S14).[24] mX in channel 1 of **3M** is rotated away from the pX orientation by 16° about the channel direction (Figure 4c), forming only one C–H···π interaction with the host—two symmetrical contacts are not possible for mX, which has a poor shape fit at long distances from the framework and unfavorable steric H···H clashes at short distances.

The reconstruction of the narrower, pocketed channel 2 is less homogeneous than that of channel 1 because more guest-specific relaxation is needed to enable xylene sorption (Figure 2d). The guest occupies the pockets defined by the good match between the length of the Ce_2 dimer and pX (Figure 4f). These pockets become more pronounced in **3P** through shape-driven relaxation of the host around the guest. The narrow region now occupied by the pX methyls extends further along the channel direction in **3P** than in **3**, whereas the wide region occupied by the guest's benzene ring is reduced in extent. Channel 2 in **3M** has similar dog-leg geometry and pocket dimensions to **3P**, but the imperfect mX fit is signaled by a guest ring hydrogen clashing with the channel surface (Figure 5c) and the guest positional disorder over two sites, in contrast to the single well-matched site occupied by pX (Figure S20).

The relaxation of channel 2 affords full xylene occupancy of the pockets for both **3P** and **3M**. In **3P** (Figure 4b) this expansion is spatially modulated to optimize the match between the channel surface chemistry and the two structural components of pX (Figure 4e,f). The guest methyl groups form two C–H···O bonds to the terminal COOH units of the

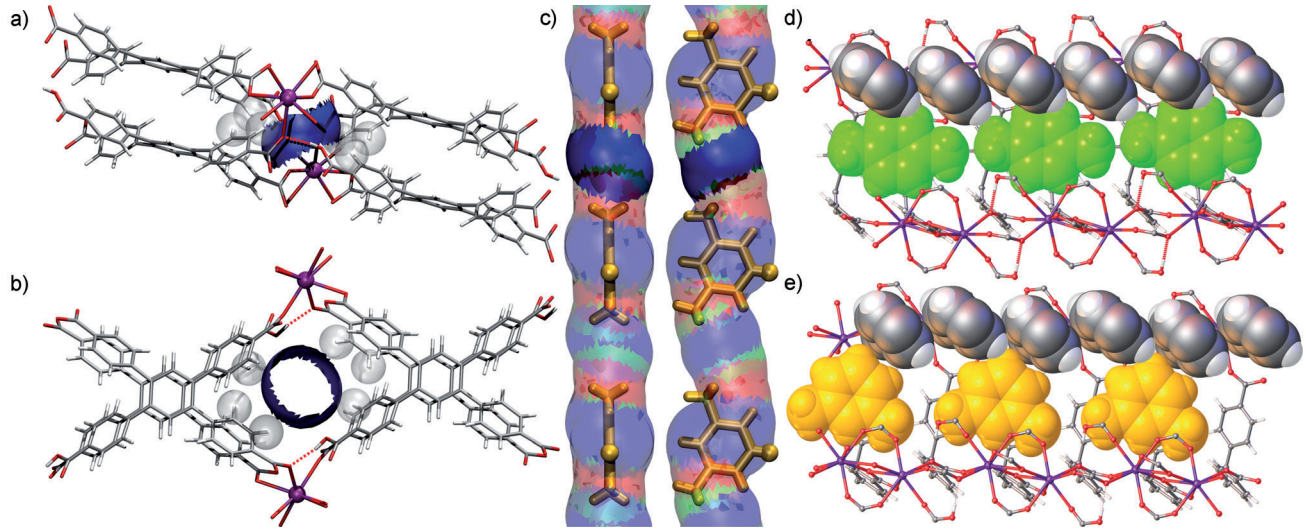

Figure 5. The guest-free expanded region in channel 2 of **3M** (highlighted in Figure 2d) shown in dark blue viewed down a) [001] and b) [100]; H12, H51, and H52 from rings 1 and 5 are represented as spheres of vdW radius. c) The pore surface of channel 2 in **3M** showing the guest-free expanded region (dark blue ring) and the location of the mX guest in orange (disorder removed); the mX methyl groups are adjacent to the guest-free expanded region and the hydrogen at the 5 position (shown as a sphere) clashes with the surface of the channel. d) Channel 2 of **3P** with pX guest (green) and the channel cut away; rings 2 and 5 of the HTCPB linker shown in a vdW depiction. e) Channel 2 of **3M** with mX guest (orange) represented as in (d).

Ce_2 dimer: these units can rotate to optimize this 3.442(6) Å interaction as carboxyphenyl ring 1 only forms a single Ce–O bond. The aromatic ring surface of the guest forms two symmetrical C–H···π interactions with hydrogen atoms on carboxyphenyl ring 4 of the linker. The mX in channel 2 of **3M** (Figure 4d) undergoes rotation and disordered positional displacement away from the pX location to minimize unfavorable close contacts to the framework (Figures S27–30). The angular disposition of the mX methyl groups permits only one weak (4.03(2) Å) C–H···O interaction and the mX C–H···π interactions are also asymmetric (Figure 4g,h). Reconstruction of channel 2 creates one optimized guest site in **3P**, but two close poorly-matched sites in **3M**, each half-occupied in the average structure.

The distortion required to accommodate mX forces the unfavorable creation of a large diameter region within channel 2 of **3M**, which is *not* occupied by any part of the mX molecule (Figure 2d), and is defined by three H atoms from rings 1 and 5 of HTCPB (Figure 5a,b). Rotation of ring 5 is driven by its close contact with hydrogen at position 5 of the mX aromatic ring (Figure 5c,e). This does not occur in **3P**, where the resulting free space is visible in Figure 5d. The carboxyphenyl ring 5 torsion angle (O58-C56-C53-C52) thus differs by 4.16° between **3P** and **3M** (Figure S32 and Table S15). Enhanced ring 1 rotation over **3P** is required to allow the COOH unit to form the single C–H···O bond in **3M**. The guest-induced rotation of rings 5 and 1 relocates their hydrogen atoms to create the guest-free expanded region.

Structural analysis reveals that **3** is not well-matched to pX or mX, and relaxes on loading to optimize capacity and fit for each guest—the superior fit to pX in **3P** is achieved with less distortion than required for the inferior match to mX in **3M**. GCMC calculations (Table S4) on the **3P** structure show that the structural relaxation from **3** doubles the capacity for pX as found experimentally, demonstrating that flexibility is essential for the observed uptake. The linker rotation observed cooperatively modifies the interactions highlighted in channels 1 (e.g. C–H···π interaction from the central benzene ring) and 2 (e.g. C–H···O interaction from carboxyphenyl ring 1). Competitive 2-component calculations give a computed thermodynamic selectivity of $\alpha_{pXmX} = 6.25$. As the initial structural match to, and the subsequent differential host relaxation around, the pX and mX guests are both involved in selection between them, variation in selectivity with lanthanide size across the family of [Ln(HTCPB)] phases (accessible for Ln = La–Sm) might be expected. The experimentally measured α_{pXmX} selectivity reaches a maximum of 6.33 at Nd(HTCPB) (Table S16). Rigid host GCMC calculations (Table S17) indicate [Ce(HTCPB)] **3** should be *more* selective than the Nd analogue, suggesting that the dynamic structural relaxation of the host around the competing guests, rather than their match to the initially rigid lattice structure, controls the extent of selectivity. Consistent with this, determination of the crystal structures of the Nd analogues **3**-Nd, **3P**-Nd and **3M**-Nd (Tables S18 and S19) reveal structural relaxation of the host on xylene loading, producing guest molecules located in very similar positions to their Ce analogues, but with smaller cell dimensions in each case. This is consistent with the reduced contact distances in the Nd materials **3P**-Nd and **3M**-Nd cooperatively amplifying both unfavorable and favorable interactions that are present in **3P** and **3M**, and thus enhancing the selectivity over that found in the Ce system because of the differential relaxation around the two guests, in contrast to calculations based on a rigid structural response of the Ce and Nd hosts. Detailed studies of desorption kinetics and cyclability will be needed to evaluate the suitability of **3** and its analogues for practical separations based on this selective sorption.

In conclusion, **3** responds flexibly to two similarly-shaped guests—it expands to enhance its capacity for pX and to admit mX, which cannot enter rigid **3** at all due to shape mismatch, to the same loading level—and yet distinguishes strongly between them despite adapting its shape to both of them because the flexible response differentiates between the two molecules. The restructuring around the preferred pX is synergic, with positive feedback between distortion of the host and enhanced fit to the guest through localized expansion and contraction. The flexibility needed to accommodate mX involves negative feedback between rearrangement to generate a compromise guest location, signaled by mX positional disorder, and the creation of unused void space remote from the guest. Nature frequently exploits conformational change of an initially mismatched biomolecule host during molecular recognition to enhance specificity.[25] This differential relaxation around similar guests is a route to high selectivity for synthetic porous solids, when larger host restructuring is needed to accommodate molecules other than the preferred target, but gives a poorer fit. This suggests that when flexible hosts are used, identification of "off-target" as well as "perfect match" structures, defined in terms of capacity for and structural fit to the preferred guest, is a valuable approach when selecting between molecules with complex shapes.

Received: August 30, 2013
Revised: December 23, 2013
Published online: March 26, 2014

Keywords: host-guest systems · metal-organic frameworks · structural rearrangement · xylenes

[1] J. R. Li, J. Sculley, H. C. Zhou, *Chem. Rev.* **2012**, *112*, 869 – 932.
[2] H.-C. Zhou, J. R. Long, O. M. Yaghi, *Chem. Rev.* **2012**, *112*, 673 – 674.
[3] C. Serre, C. Mellot-Draznieks, S. Surble, N. Audebrand, Y. Filinchuk, G. Ferey, *Science* **2007**, *315*, 1828 – 1831.
[4] S. Horike, S. Shimomura, S. Kitagawa, *Nat. Chem.* **2009**, *1*, 695 – 704.
[5] a) T. K. Maji, R. Matsuda, S. Kitagawa, *Nat. Mater.* **2007**, *6*, 142 – 148; b) S. B. Choi, H. Furukawa, H. J. Nam, D. Y. Jung, Y. H. Jhon, A. Walton, D. Book, M. O'Keeffe, O. M. Yaghi, J. Kim, *Angew. Chem.* **2012**, *124*, 8921 – 8925; *Angew. Chem. Int. Ed.* **2012**, *51*, 8791 – 8795.
[6] A. Corma, *Chem. Rev.* **1995**, *95*, 559 – 614.
[7] D. Peralta, G. Chaplais, A. Simon-Masseron, K. Barthelet, G. D. Pirngruber, *Ind. Eng. Chem. Res.* **2012**, *51*, 4692 – 4702.
[8] a) Y.-S. Bae, C. Y. Lee, K. C. Kim, O. K. Farha, P. Nickias, J. T. Hupp, S. T. Nguyen, R. Q. Snurr, *Angew. Chem.* **2012**, *124*, 1893 – 1896; *Angew. Chem. Int. Ed.* **2012**, *51*, 1857 – 1860; b) E. D. Bloch, W. L. Queen, R. Krishna, J. M. Zadrozny, C. M. Brown, J. R. Long, *Science* **2012**, *335*, 1606 – 1610.
[9] Z. R. Herm, B. M. Wiers, J. A. Mason, J. M. van Baten, M. R. Hudson, P. Zajdel, C. M. Brown, N. Masciocchi, R. Krishna, J. R. Long, *Science* **2013**, *340*, 960 – 964.
[10] a) H. Hayashi, A. P. Cote, H. Furukawa, M. O'Keeffe, O. M. Yaghi, *Nat. Mater.* **2007**, *6*, 501 – 506; b) P. Serra-Crespo, M. A. van der Veen, E. Gobechiya, K. Houthoofd, Y. Filinchuk, C. E. A. Kirschhock, J. A. Martens, B. F. Sels, D. E. De Vos, F. Kapteijn, J. Gascon, *J. Am. Chem. Soc.* **2012**, *134*, 8314 – 8317.
[11] H. Sato, W. Kosaka, R. Matsuda, A. Hori, Y. Hijikata, R. V. Belosludov, S. Sakaki, M. Takata, S. Kitagawa, *Science* **2013**, *343*, 167 – 170.
[12] J.-P. Bellat, M.-H. Simonot-Grange, S. Jullian, *Zeolites* **1995**, *15*, 124 – 130.
[13] a) P. S. Bárcia, D. Guimaraes, P. A. P. Mendes, J. A. C. Silva, V. Guillerm, H. Chevreau, C. Serre, A. E. Rodrigues, *Microporous Mesoporous Mater.* **2011**, *139*, 67 – 73; b) Z. Y. Gu, X. P. Yan, *Angew. Chem.* **2010**, *122*, 1519 – 1522; *Angew. Chem. Int. Ed.* **2010**, *49*, 1477 – 1480.
[14] L. Alaerts, M. Maes, L. Giebeler, P. A. Jacobs, J. A. Martens, J. F. M. Denayer, C. E. A. Kirschhock, D. E. De Vos, *J. Am. Chem. Soc.* **2008**, *130*, 14170 – 14178.
[15] R. El Osta, A. Carlin-Sinclair, N. Guillou, R. I. Walton, F. Vermoortele, M. Maes, D. de Vos, F. Millange, *Chem. Mater.* **2012**, *24*, 2781 – 2791.
[16] V. Finsy, C. E. A. Kirschhock, G. Vedts, M. Maes, L. Alaerts, D. E. De Vos, G. V. Baron, J. F. M. Denayer, *Chem. Eur. J.* **2009**, *15*, 7724 – 7731.
[17] a) G. Sheldrick, *Acta Crystallogr. Sect. A* **2008**, *64*, 112 – 122; b) O. V. Dolomanov, L. J. Bourhis, R. J. Gildea, J. A. K. Howard, H. Puschmann, *J. Appl. Crystallogr.* **2009**, *42*, 339 – 341.
[18] O. K. Farha, K. L. Mulfort, J. T. Hupp, *Inorg. Chem.* **2008**, *47*, 10223 – 10225.
[19] J. Rouquerol, F. Rouquerol, K. S. W. Sing, *Adsorption by Powders and Porous Solids: Principles*, Academic Press, London, **1999**.
[20] a) G. R. Desiraju, T. Steiner, *The Weak Hydrogen Bond: In Structural Chemistry and Biology*, Oxford University Press, Oxford, **2001**; b) S. K. Burley, G. A. Petsko, *Science* **1985**, *229*, 23 – 28; c) S. Tsuzuki, *Struct. Bonding (Berlin)* **2005**, *115*, 149 – 193.
[21] L. Alaerts, C. E. A. Kirschhock, M. Maes, M. A. van der Veen, V. Finsy, A. Depla, J. A. Martens, G. V. Baron, P. A. Jacobs, J. E. M. Denayer, D. E. De Vos, *Angew. Chem.* **2007**, *119*, 4371 – 4375; *Angew. Chem. Int. Ed.* **2007**, *46*, 4293 – 4297.
[22] J.-P. Bellat, M.-H. Simonot-Grange, *Zeolites* **1995**, *15*, 219 – 227.
[23] F. Vermoortele, M. Maes, P. Z. Moghadam, M. J. Lennox, F. Ragon, M. Boulhout, S. Biswas, K. G. M. Laurier, I. Beurroies, R. Denoyel, M. Roeffaers, N. Stock, T. Duren, C. Serre, D. E. De Vos, *J. Am. Chem. Soc.* **2011**, *133*, 18526 – 18529.
[24] S. K. Wolff, D. J. Grimwood, J. J. McKinnon, M. J. Turner, D. Jayatilaka, M. A. Spackman, CrystalExplorer, Version 3.0, **2012**.
[25] Y. Savir, T. Tlusty, *Plos One* **2007**, *2*, e468.
[26] O. S. Smart, J. M. Goodfellow, B. A. Wallace, *Biophys. J.* **1993**, *65*, 2455 – 2460.

